

Magnetorheological semi-active mount system for engines: Prototyping and testing

Qing Liu^{1,2*}, Guo-Dong Bai^{1*}, Zhi-Hao Liu³, Xian-Xu ‘Frank’ Bai¹ ,
 Hao Du¹, Peng Chen¹ and Li-Jun Qian¹

Abstract

In order to maximize the controllability of magnetorheological (MR) mount for engines, a novel (MR) mount with an internal bypass (MRM-IB), which provides particular advantages of large dynamic stiffness range, small field-off dynamic stiffness and long available stroke under full vibration frequency range, is proposed and investigated in this paper. The proposed MRM-IB consists of a main rubber spring unit for supporting static load and a MR damping unit for mechanical energy dissipation. The MR damping unit is composed of a piston assembly, a MR fluid chamber and an annular MR fluid channel sandwiched by two concentric cylinders, that is, the inner and outer cylinders. Electromagnetic coil winding is wound on the outside of the inner cylinder and continuous damping/dynamic stiffness of the MRM-IB is tuned by the applied current in the coils. Structural principle of the magnetic circuit of the proposed MRM-IB is validated and analyzed, and the mathematical model of the controllable damping force is then established. In addition, a frequency-based piecewise controller and a fuzzy controller for a specific MR semi-active automotive mount system are designed, and the theoretical simulation and the experimental tests of the system are conducted, compared and analyzed.

Keywords

Magnetorheological (MR) fluids, magnetorheological (MR) mount, internal bypass valve, dynamic stiffness, engine, vibration frequency

Date received: 23 January 2020; accepted: 20 April 2020

Introduction

Magnetorheological (MR) mounts are a typical application of MR fluids.^{1–5} MR mounts with different structures and performances have been applied in various vibration control systems^{6–19} and have been a hot research topic that has attracted worldwide attentions. A squeeze-flow hybrid mode MR mount was designed, optimized and tested by Elahinia’s group.^{9,10} The dynamic stiffness changes uniformly under full working frequency range as the excitation magnetic field changes and the vibration transmissibility from the automotive engine to the body is greatly reduced with a skyhook controller. Structural optimization and vibration isolation control performance of another MR mount was conducted for a variable throttle engine by Mansour et al.¹² In 2014, Choi’s group proposed a shear-flow hybrid mode MR mount.¹³ Nondimensional model of the MR mount based on the constitutive equations was developed, and further the nondimensional parameters of the model were analyzed for the MR mount design. To meet the requirement of large controllable damping

force in diesel engine mount system, Choi’s group proposed and optimized a MR mount with an annular-disk duct.^{14,15} Later, a novel hybrid mount with air spring and MR damper with an indirect fuzzy-sliding mode controller for vibration isolation of a heavy precision stage was further investigated.^{16,17} Under the collaboration, Guo’s group¹⁸ and Farjoud et al.¹⁹ established and

¹Laboratory for Adaptive Structures and Intelligent Systems (LASIS), Department of Vehicle Engineering, Hefei University of Technology, Hefei, People’s Republic of China

²Tai’an Special Vehicle Co., Ltd., Tai’an, People’s Republic of China

³Xi’an Research Institute of High Technology, Xi’an, People’s Republic of China

*The first two authors Qing Liu and Guo-Dong Bai contributed equally to this work.

Corresponding author:

Xian-Xu ‘Frank’ Bai, Laboratory for Adaptive Structures and Intelligent Systems (LASIS, www.lasiser.com), Department of Vehicle Engineering, Hefei University of Technology, Hefei 230009, People’s Republic of China.
 Email: bai@hfut.edu.cn

verified a steady-state model of a squeeze-mode MR mount with the consideration of the responses of the MR fluids in squeeze mode, fluid viscosity, and fluid inertia. As for the automotive engine mount system featuring wide-band vibration frequency, we proposed, designed and developed a novel unidirectional MR squeeze mount fulfilled with only 22 mL MR fluids,^{20,21} which would significantly reduce the cost of MR mount system. The dynamic behavior of the MR fluids working in squeeze mode was thoroughly investigated, and the conclusion that under high-frequency oscillatory excitation, squeeze-strengthen effect found in quasi-static state does not occur was obtained. Based on Bingham model of MR fluids, the mathematical model and analysis of large controllable damping force with small amplitudes, which exists in MR squeeze mount, was carried out by Sapiński and Snamina.²² They emphasized the quasi-static mechanical properties of MR squeeze mount.

However, the conventional MR mounts with damping holes or inertia channel would be blocked when under high-frequency excitations. Although the decouplers are employed, fluidic resonance will still increase the field-off dynamic stiffness of the conventional MR mounts. At the same time, the controllability of the damping force is limited due to the block of the damping hole or inertia channel. What is more, the conventional MR mounts require a large amount of MR fluids because of the large fluid chamber, which will further increase the cost. We have tried to design a MR mount in squeeze mode, but the controllability is limited by the squeeze gap. The application of the squeeze MR mounts therefore is seriously limited.^{20,21}

Based on the review above, to solve the issue of the existing techniques and maximize the controllability of MR mounts for engines, a new structure of MR mount with an internal bypass (MRM-IB) is proposed. It is featuring a large dynamic stiffness range, small field-off dynamic stiffness and long working stroke under the full vibration frequency range. The finite element entity of the MRM-IB is established to verify the structural principle via static electromagnetic field simulation. The mathematical model of the controllable damping force of the MRM-IB is then established. Further, a frequency-based piecewise controller and a fuzzy controller are designed for the MR mount system according to the vibration characteristics of engines. The comparison and analysis of the MR mount control system are conducted via simulation and prototype testing.

Structure and principle of the proposed MRM-IB

Structural principle

Figure 1(a)–(c) present the principle, three-dimensional drawing and parts of the proposed MRM-IB, respectively. As shown in Figure 1, the proposed MRM-IB is composed of a main rubber spring unit and a MR damping unit. The main rubber spring unit is set

outside of the MR fluid chamber to support static loads. The MR damping unit is composed of a piston assembly, a MR fluid chamber and an annular MR fluid channel sandwiched by two concentric cylinders (i.e. the inner and outer cylinders). Axial motion of the piston assembly along the inner cylinder leads to the flow of MR fluids inside the annular MR fluid channel and inner cylinder, which induces the parallel action of the piston assembly and MR damping unit. So that, MR fluids in the annular channel work in pure flow mode. Continuously controllable damping/stiffness can be realized by adjusting the applied current in the electromagnetic coil winding, which are wound around the annular groove of the inner cylinder. Specific advantages of the proposed MRM-IB are that (1) the MRM-IB maximizes the MR effect area and large ranges of controllable damping/stiffness can then be provided, (2) the MRM-IB maintains small field-off dynamic stiffness in high frequencies because of large enough MR fluid channel, and (3) the coil-piston structures of the conventional MR mounts are updated with the decoupled one, which realizes a large stroke of the MRM-IB.

Finite element analysis of the static electromagnetic field

Figure 2(a) and (b) present the magnetic flux lines and magnetic field distribution along the MR fluid channel under 2.0 A applied current. As shown in Figure 2(a), the magnetic flux lines of the MRM-IB form a closed loop along the inner and outer cylinders. They totally pass through the MR fluid channel between the inner and outer cylinders. It is seen from Figure 2(b) that the magnetic flux density generated by the electromagnetic coil winding shows a certain relationship with the magnitude of the applied current. The larger the applied current is, the stronger the magnetic flux density will be. The magnetic flux density can be realized in the range of 0–0.4 T, which will be good for the controllability.

Force model

Considering the damping force caused by the MR effect, viscosity effect and inertia effect, the output force F of the MRM-IB can be expressed by

$$F = \Delta P \cdot A_p + F_s \quad (1)$$

$$\Delta P = \Delta P_\tau + \Delta P_\eta + \Delta P_I \quad (2)$$

where ΔP is the total pressure drop through the piston of the MRM-IB; F_s is the force of the main rubber spring; ΔP_τ is the pressure drop caused by the MR effect; ΔP_η is the pressure drop caused by the viscosity effect; ΔP_I is the pressure drop caused by the inertia effect; and A_p represents the effective area of the piston. The pressure drop caused by the MR effect is given by²³

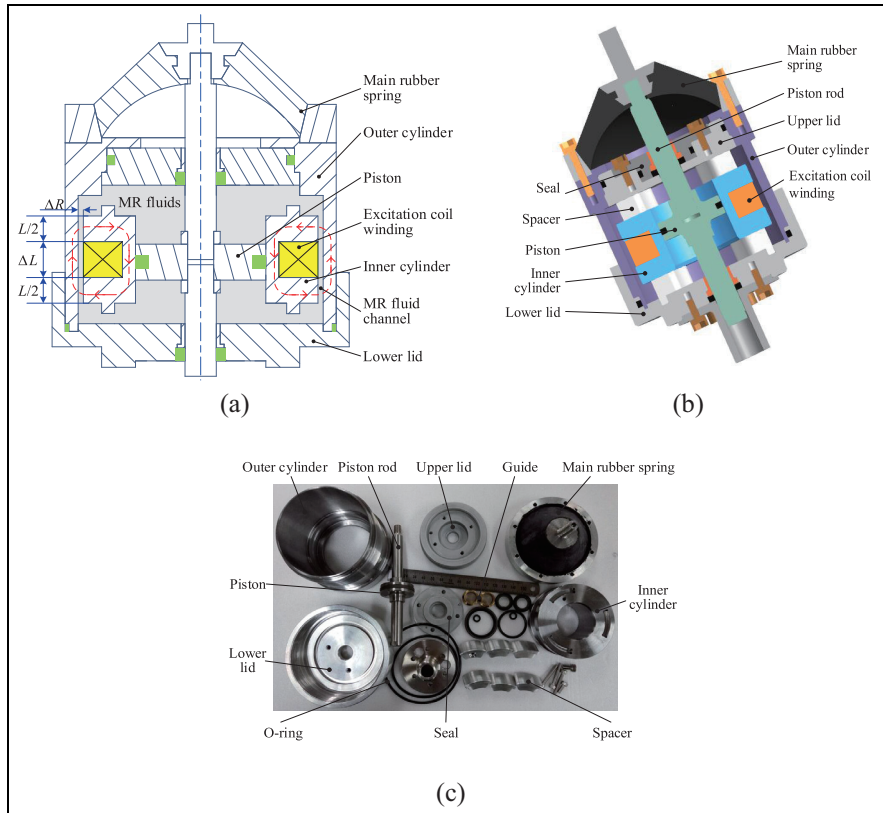


Figure 1. Structure of the proposed MRM-IB: (a) principle, (b) three-dimensional drawing, and (c) parts.

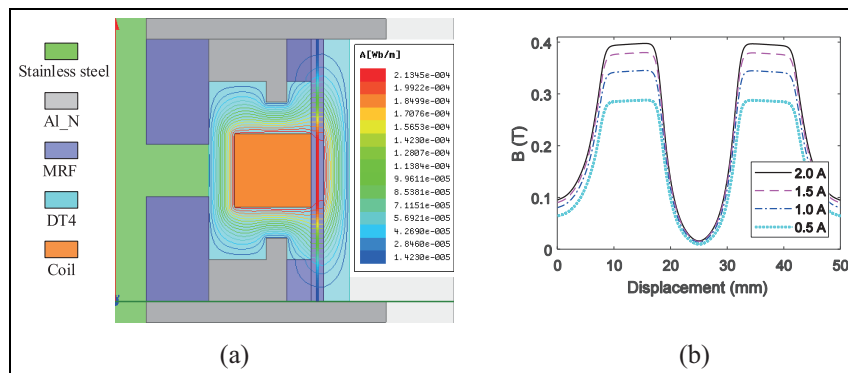


Figure 2. Finite element analysis results of the proposed MRM-IB with a 2.0 A applied current in the coils: (a) magnetic flux lines and (b) magnetic flux density along the MR fluid channel.

$$\Delta P_\tau = \frac{2L\tau_y}{\Delta R} \quad (3)$$

$$\begin{aligned} \tau_y = & -103.1 \times B^4 + 118.9 \times B^3 - 17.85 \times B^2 \\ & + 48.94 \times B - 2.636 \end{aligned} \quad (4)$$

where L and ΔR , respectively, represent the length and width of the MR fluid channel, which is shown in Figure 1(a); \dot{x}_r is the flow velocity of MR fluids in the channel; and τ_y is the shear yield stress of MR fluids which is dependent on the magnetic flux density. As seen from Figure 3, the experimental relationship between the shear yield stress and magnetic flux density of a commercially available MR fluids MRF-132DG is fitted as

where B is the magnetic flux density.

Viscous pressure drop can be expressed by²⁴

$$\Delta P_\eta = \frac{6(L + \Delta L)\eta}{(\Delta R)^2} \dot{x}_r \quad (5)$$

where ΔL is the width of the electromagnetic coil winding and η is the field-off viscosity of MR fluids.

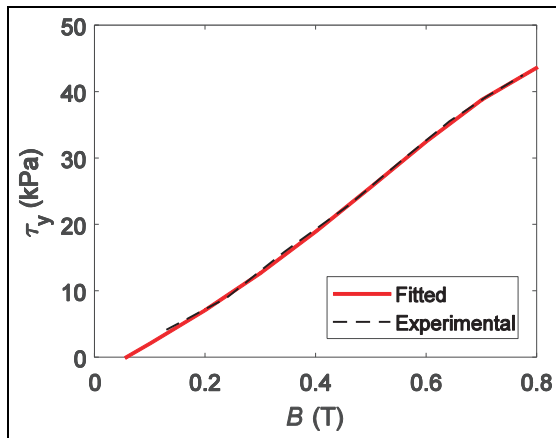


Figure 3. Shear yield stress versus magnetic flux density of the MR fluids.

Inertial pressure drop is given by

$$\Delta P_I = (L + \Delta L)\rho\ddot{x}_r \quad (6)$$

where ρ represents the density of MR fluids and \ddot{x}_r represents the acceleration of MR fluids in the channel.

Tests of the developed MRM-IB

Static and dynamic mechanical properties of the developed MRM-IB using a Servo-hydraulic Test System (Type: MTS Landmark) shown in Figure 4 are experimentally tested. The upper and lower ends of the MRM-IB are fixed in between the upper actuator and lower force sensor in test system, respectively. A displacement sensor is installed along the upper actuator. When the upper actuator moves, the mechanical response versus displacement/velocity of the MRM-IB can be obtained. The Servo-hydraulic Test System will provide quasi-static and dynamic sinusoidal displacement excitations.

Static stiffness

A velocity of 5 mm/min excitation is provided by the test system as shown in Figure 4. Figure 5 shows the force-displacement curves of the developed MRM-IB. The developed MRM-IB provides a quite linear stiffness as seen from the figure. Fitting the force-displacement results of the loading and unloading conditions, the average value of 79 N/mm of the static stiffness is obtained.

Frequency response in field-off state

Frequency response of the MRM-IB contains the performances of the main rubber spring unit and the MR damping unit. The MRM-IB with no MR fluids is tested for the response of the main rubber spring unit, while the field-off dynamic stiffness is obtained from the tests of the MRM-IB fulfilled with MR fluids.

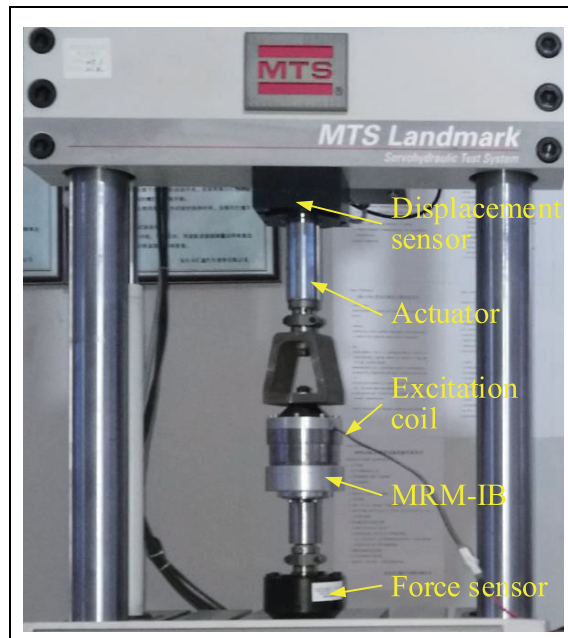


Figure 4. Mechanical property test system for the developed MRM-IB.

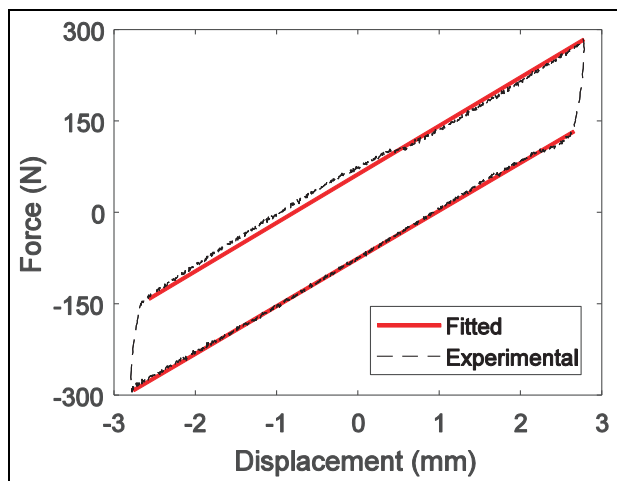


Figure 5. Force-displacement curves of the developed MRM-IB under static loads.

Figure 6 presents the experimental tests in profile of force versus displacement when the main rubber spring under sinusoidal displacement excitation with an amplitude of 1.0 mm and different frequencies. Observing Figure 6, the main rubber spring does not get strengthened with the increase of the frequency. In other words, the dynamic stiffness of the MRM-IB is insensitive to frequency.

Figure 7(a) and (b) present the experimental field-off tests in profile of force versus displacement when the developed MRM-IB under sinusoidal displacement excitation with amplitudes of 1.0 and 0.1 mm, respectively. As shown in Figure 7(a) and (b), limited influence of the excitation frequency on the mechanical

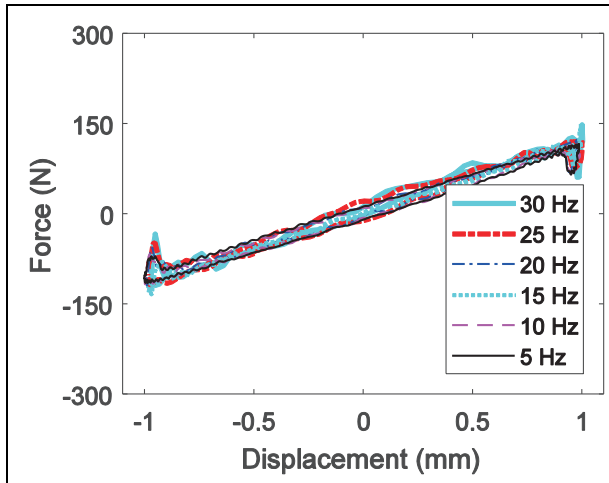


Figure 6. Force-displacement curves of the main rubber spring of the developed MRM-IB under sinusoidal displacement excitation with different frequencies.

properties of the developed MRM-IB at field-off state can be found. It means that low field-off dynamic stiffness remains in high frequencies. In contrast, the excitation displacement has a great effect on the field-off mechanical properties of the developed MRM-IB. The reason is that the flow magnitude of the MR fluids in the channel is determined by the excitation displacement. When under small displacement excitations, the field-off damping force decreases, which is caused by the reduction of the flow magnitude. In addition, comparing Figures 6 and 7(a), the influence of the viscosity and inertia properties on the mechanical characteristics of the developed MRM-IB cannot be ignored.

Controllable damping force

Figure 8(a)–(c) present the experimental results in profile of force versus displacement when under 10 Hz sinusoidal displacement excitation with different amplitudes and applied currents. As shown in Figure 8(a), when under the excitation with an amplitude of 1 mm,

the peak damping force and the area enclosed by the force versus displacement curve both increase with the applied current. Controllable damping property is realized. According to Figure 8(b) and (c), when under small displacement excitations, the peak damping force drops due to the MR effect. In order to realize a low field-off dynamic stiffness, the width of the MR fluid channel is set as large as 2.3 mm. Therefore, when the excitation amplitude is small and the pressure drops increases with the applied current, the flow magnitude in the MR fluid channel decreases, so that the range of controllable damping force becomes small.

Controllable dynamic stiffness

For the engine mount system, the equivalent dynamic stiffness is more often used instead of the damping force. Figure 9(a)–(c) present the equivalent controllable dynamic stiffness of the developed MRM-IB variations with excitation frequency and applied current when under sinusoidal displacement excitation with amplitudes of 1.0, 0.5, and 0.1 mm, respectively. As shown in Figure 9(a), the dynamic stiffness of the developed MRM-IB nonlinearly increases with the applied current and is little affected by the excitation frequency. Comparing Figure 9(a)–(c), the dynamic stiffness increases as excitation displacement drops on the premise that the applied current and excitation frequency remain unchanged. Besides, the controllability of the dynamic stiffness caused by the MR effect drops a little, and the increase of the dynamic stiffness under larger current is lower than the smaller one. One possible reason is that the hysteresis properties lead to the insufficient excitation displacement under small amplitude excitation.²⁵ Thus, a large controllable dynamic stiffness is induced.

Equivalent damping

Figure 10(a)–(c) present the equivalent damping of the developed MRM-IB variations with the excitation frequency and the applied current when under sinusoidal

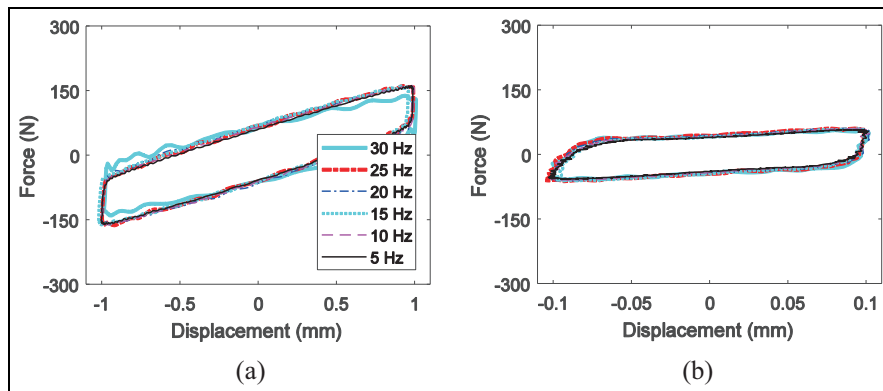


Figure 7. Field-off damping force-displacement curves of the developed MRM-IB under sinusoidal displacement excitation with different frequencies and amplitudes: (a) 1.0 mm and (b) 0.1 mm.

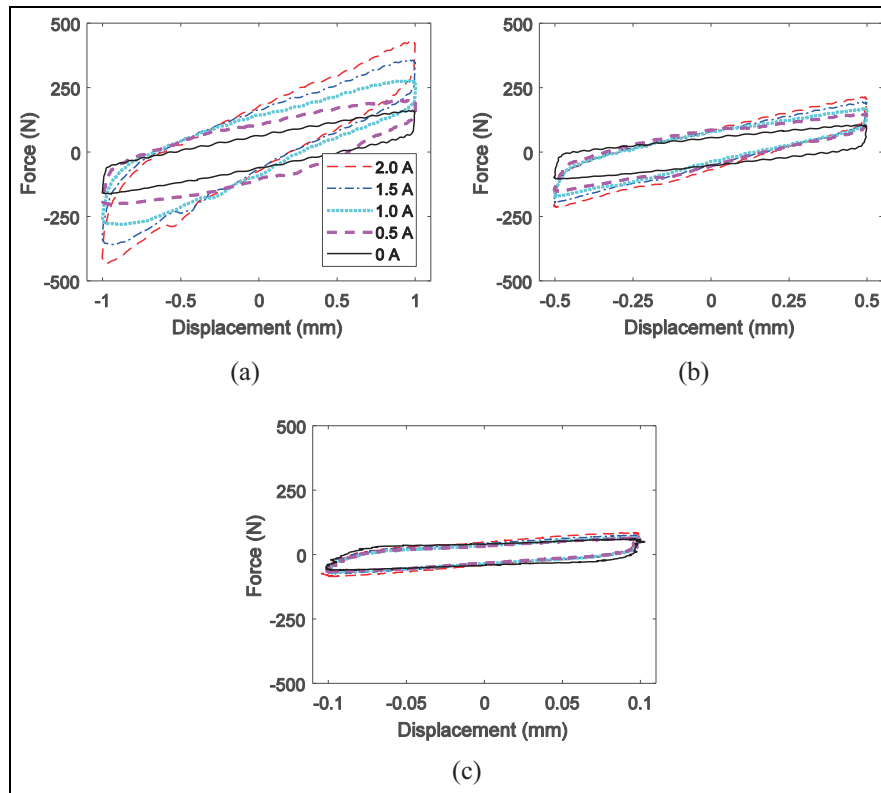


Figure 8. Force-displacement curves of the developed MRM-IB under 10 Hz sinusoidal displacement excitation with different amplitudes: (a) 1.0 mm, (b) 0.5 mm, and (c) 0.1 mm.

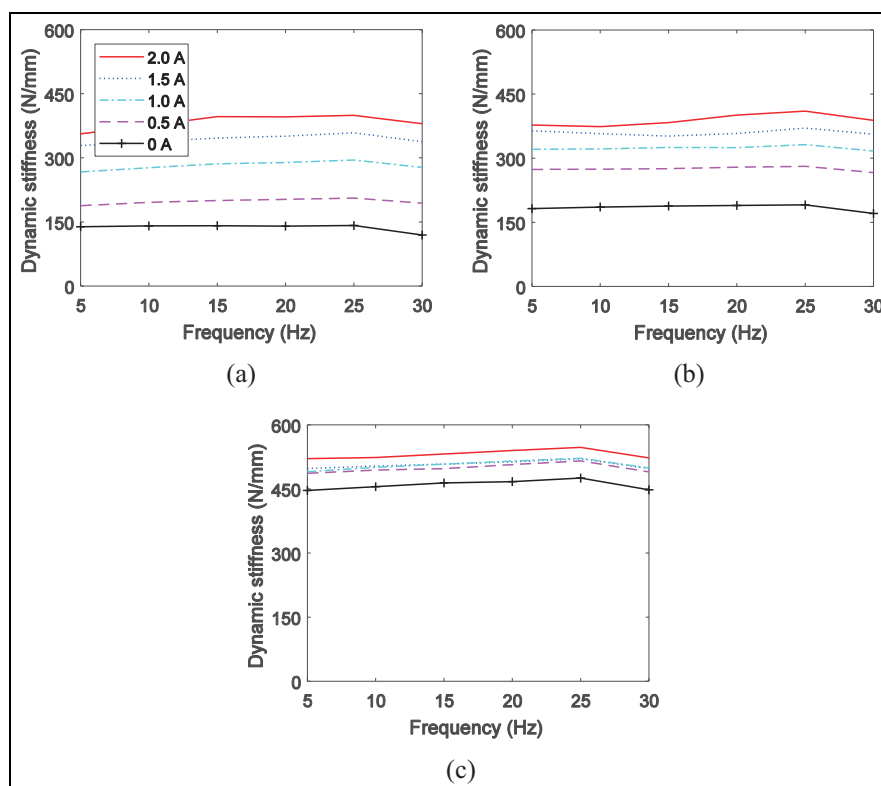


Figure 9. Dynamic stiffness of the developed MRM-IB under sinusoidal displacement excitation with different amplitudes: (a) 1.0 mm, (b) 0.5 mm, and (c) 0.1 mm.

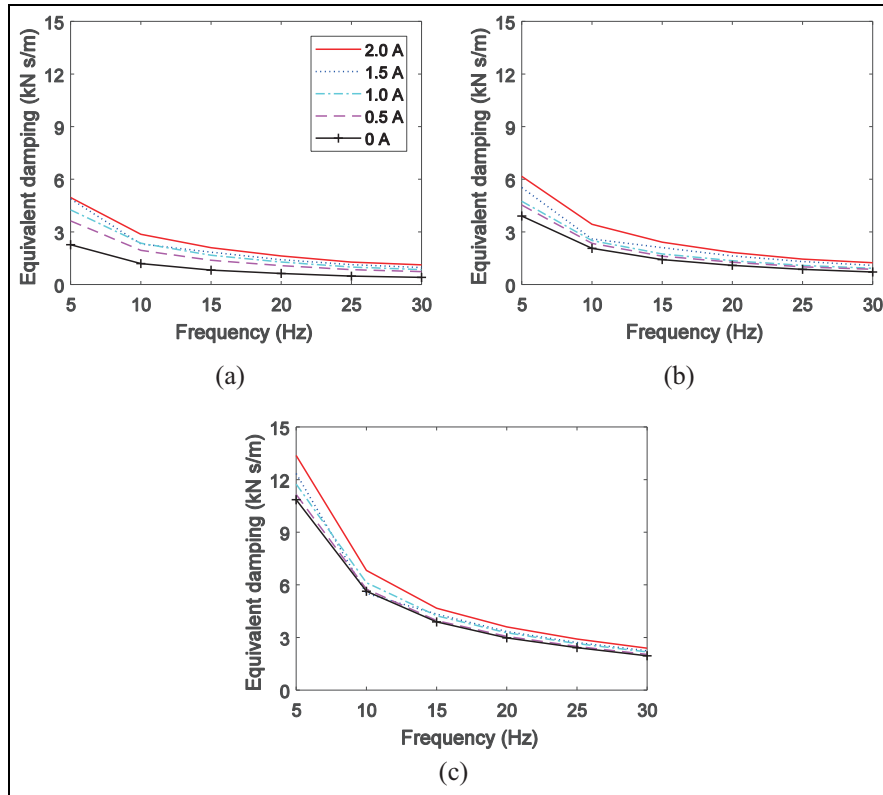


Figure 10. Equivalent damping of the developed MRM-IB under sinusoidal displacement excitation with different amplitudes: (a) 1.0 mm, (b) 0.5 mm, and (c) 0.1 mm.

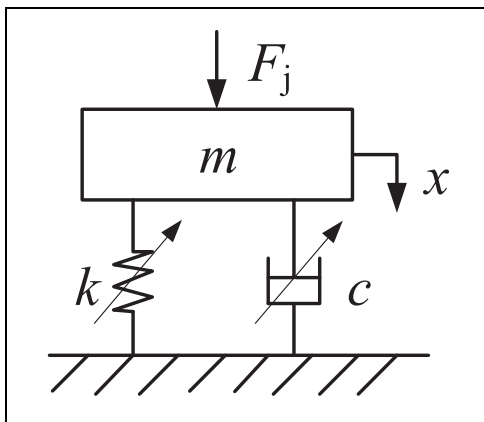


Figure 11. Single degree of freedom model of the engine mount system for vibration isolation.

displacement excitation with amplitudes of 1.0, 0.5, and 0.1 mm, respectively. According to Figure 10, the equivalent damping of the developed MRM-IB nonlinearly increases with the applied current. When over 20 Hz, the effect of the applied current on equivalent damping is weakened. The equivalent damping nonlinearly drops with the increase of the frequency. Comparing Figure 10(a)–(c), when the applied current and the excitation frequency remain unchanged, the smaller the excitation amplitude, the bigger the equivalent damping.

Controller design for the MRM-IB based engine mount system

Vertical excitation force from engines

The schematic of the vertical dynamics of a single-cylinder engine is shown in Figure 11. The resultant force F_j can be simplified as the reciprocating inertial force Q_Z on the piston pin and the rotating inertial force Q_{rV} on the crankshaft pin. It is expressed by

$$F_j = Q_Z + Q_{rV} = -m_j r \omega^2 \cos \omega t - m_j r \lambda \omega^2 \cos 2\omega t + m_r r \omega^2 \cos \omega t \quad (7)$$

where m_j is the equivalent mass converted to the piston pin, m_r is the equivalent mass converted to the crankshaft pin, r is the length of the crankshaft, λ is the length ratio of the crankshaft to the connecting rod, ω is the angular speed of the rotating crankshaft, and t is the time.

The dynamic model of the engine vibration isolation system using the MRM-IB can be expressed by

$$m\ddot{x} = F_j - cx - kx \quad (8)$$

where m represents the engine mass; c represents the equivalent damping of the MRM-IB; k represents the stiffness of the MRM-IB; and x , \dot{x} and \ddot{x} stand for the vibration displacement, velocity and acceleration of the engine, respectively.

Table I. Fuzzy control rules.

f_2	$ a $	PZ	PS	PM	PB	PL
PZ		PL	PL	PB	PB	PM
PS		PL	PB	PB	PM	PM
PM		PB	PM	PM	PS	PS
PB		PM	PM	PS	PS	PZ
PL		PM	PS	PS	PZ	PZ

PZ: zero; PS: positive small; PM: positive medium; PB: positive big; PL: positive large.

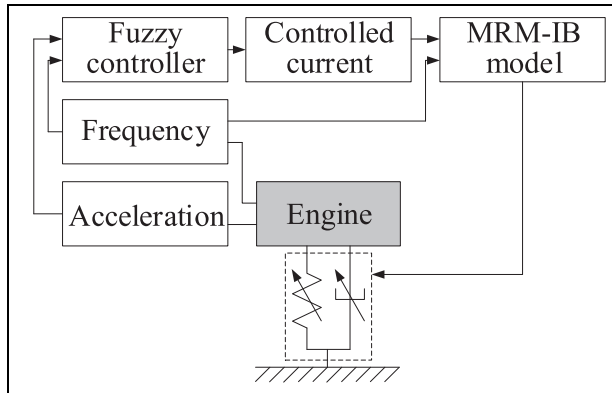


Figure 12. Schematic of the MRM-IB based engine vibration isolation using fuzzy controller.

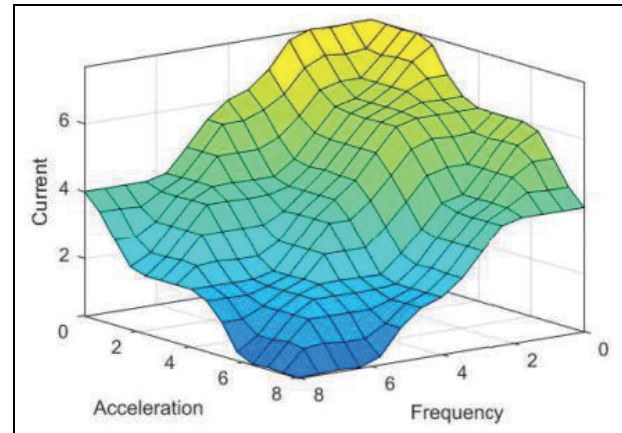


Figure 13. Surface of the fuzzy control rules.

Fuzzy controller

The dynamic properties of the single-cylinder engine are measured on the experimental setup of the engine mount system. The second-order frequency f_2 ($=2f$, f is the main frequency) is within 8.33–43.33 Hz. The acceleration of the engine at the mount side varies from -20 to 20 m/s^2 . In addition, the controlled signal of the applied current i of the developed MRM-IB is set within 0–2 A.

The schematic of the fuzzy control system for the engine vibration isolation is shown in Figure 12. Using the measured dynamic responses of the engine mount system, the second-order frequency f_2 of the engine and the absolute value of the acceleration $|a|$ of the engine at the mount side are selected as the input variables of the designed fuzzy controller. The output variable is the applied current i .

The basic discourses of the second-order frequency f_2 , the absolute value of the acceleration $|a|$ of the engine at the mount side and the applied current i are [13,45], [0, 20] and [0, 2], respectively. They can be converted to the universes of the fuzzy sets $\{0, 1, 2, 3, 4, 5, 6, 7, 8\}$. The variables in the system can be subdivided into a range of states: PZ, PS, PM, PB, and PL, where PZ represents “zero,” PS represents “positive small,” PM represents “positive medium,” PB represents “positive big,” and PL represents “positive large.” The quantization factor of the second-order frequency k_f and the absolute value of the acceleration of the engine at the

mount side k_a are $8/43.33$ and $8/20$, respectively. The proportion factor of the applied current k_i is $2/8$. Mamdani max-min inferencing is selected for the purpose of fuzzy inference decision, and the method of the center of gravity is used for defuzzification.

Triangular, zigzag and sigmoidal membership functions are selected as the inputs, and triangular membership function is used as the output. The fuzzy control rules as listed in Table 1 are established after analyzing the influence of the excitation frequency and the acceleration on the engine vibration. In addition, the surface of the fuzzy control rules is also presented in Figure 13.

Frequency based piecewise controller

Based on considerable experimental tests of the single-cylinder engine, the principle of the frequency-based piecewise controller is proposed and presented in Figure 14. The frequency-based piecewise controller is proposed in the light of the different requirements of the developed MRM-IB for vibration isolation when under different excitation frequencies. In other words, the dynamic characteristics of the MRM-IB are adjusted real-timely according to the vibration frequency of the engine, which will realize simple and efficient suppression of the engine vibration.

Based on the characteristics of the single-cylinder engine, the startup, idle, and maximum rotational

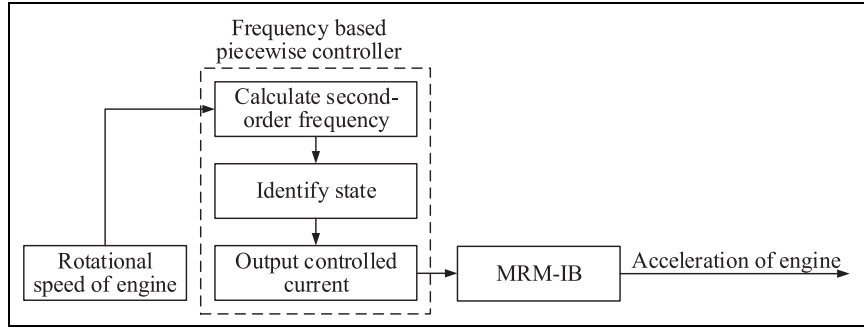


Figure 14. Principle of the frequency based piecewise controller.

Table 2. Frequency based piecewise control rules.

Rotational speed (r/min)	Second-order frequency (Hz)	Controlled current (A)
500–1600	8.33–26.67	2.0
1600–2100	26.67–35	1.0
2100–2600	35–43.33	0.5

speeds are 500, 800, and 2600 r/min, respectively. So the range of the rotational speed is 500–2600 r/min. The corresponding second-order frequency is in a range of 8.33–43.33 Hz. The strategy of the frequency-based piecewise control is listed in Table 2. As seen from Table 2, the higher the frequency, the smaller the applied current provided to the MRM-IB.

Preliminary control comparison

The established mathematical model is analyzed under the conditions of 800 r/min for the idle speed, 1400 r/min for the low speed, 1800 r/min for the medium speed

and 2200 r/min for the high speed. Figure 15(a)–(d) present the time-domain acceleration in the conditions of 800, 1400, 1800, and 2200 r/min, respectively. Frequency response of the acceleration is shown in Figure 16. As compared with the passive state (i.e. the control off state), under the two semi-active controllers (i.e. fuzzy controller and frequency-based piecewise controller), the vibration is significantly isolated via the MRM-IB. Furthermore, the frequency-based piecewise controller even better than the fuzzy controller for reducing the peak at the second-order frequency.

Tests of the MRM-IB based engine vibration isolation control system

Test bench

The test bench for the MRM-IB based single-cylinder engine vibration isolation control system is built and shown in Figure 17. As seen from the figure, the engine is fixed on three struts, that is, two passive rubber springs and a MRM-IB. The MRM-IB and its control

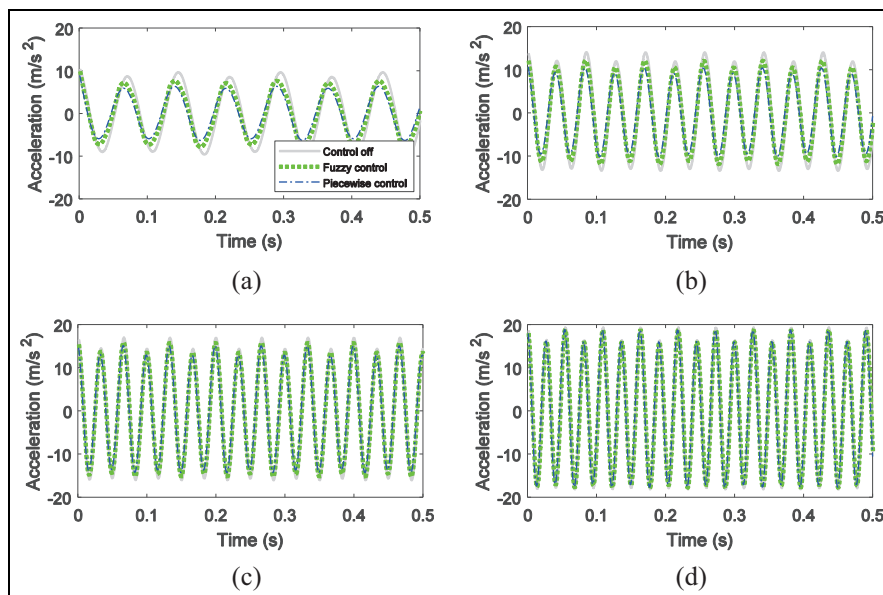


Figure 15. Simulation results of the time histories of the acceleration: (a) 800 r/min, (b) 1400 r/min, (c) 1800 r/min, and (d) 2200 r/min.

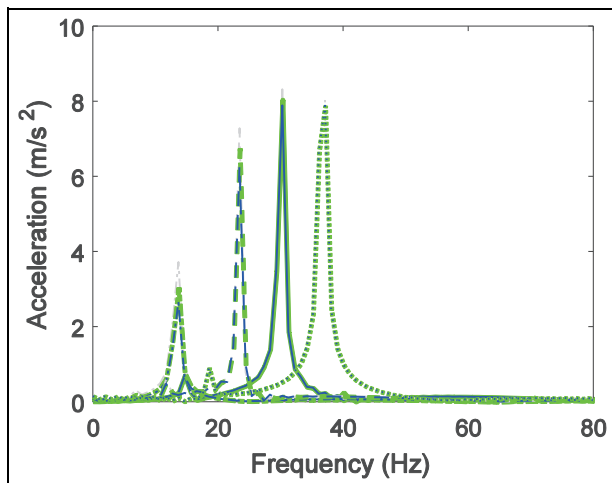


Figure 16. Simulation results of the frequency response of the accelerations when under different strategies and rotational speeds.

Note: Dash-dot line - 800 r/min; Dashed line - 1400 r/min; Solid line - 1800 r/min; and Dotted line - 2200 r/min. Grey - Control off; Green - Fuzzy control; Blue - Piecewise control.

system are added to the engine mount system, including a rotational speed transducer, an accelerometer, a controller, and a current driver. The accelerometer is installed at the engine to measure the vertical vibration. The rotational speed transducer installed at the flywheel side is utilized to collect the engine speed. According to the control algorithm and engine vibration, the developed controller outputs the commands to the current driver to tune the mechanical output of the MRM-IB in real time. DEWE-501 is used for all the data acquisition.

Results

Figure 18(a)–(d) show the time response of the acceleration of the engine at the MRM-IB side under the rotational speeds of 800, 1400, 1800, and 2200 r/min, respectively. As shown in Figure 18, vibration frequency increases with the rotational speed. The MRM-IB shows better control performance at low frequencies than at high ones. Observing Figure 18(b), as compared with the passive state in Figure 18(a), the MRM-IB provides more significant vibration isolation performance at low frequencies with any controller. In addition, the results of the frequency-based piecewise controller are better than the fuzzy controller. Combining Figure 18(a)–(d), the effects of the vibration isolation with controllers decrease at medium frequencies and almost similar with the passive state at high frequencies. At the same time, the results of the frequency-based piecewise controller are better than fuzzy controller at medium and high frequencies again.

Figure 19 presents the experimental tests of the frequency response of the acceleration. As compared with the passive state, both the piecewise controller and fuzzy controller significantly reduce the peak of the

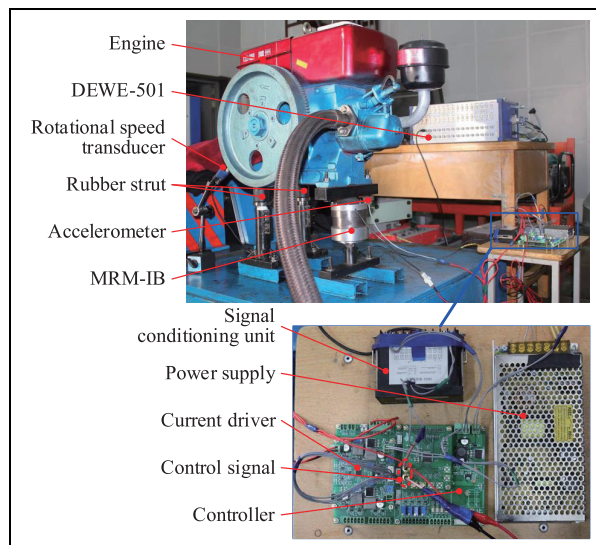


Figure 17. Prototype of the test bench of the MRM-IB based engine vibration isolation control system.

second-order frequency of the acceleration. As the frequency increases, the control effectiveness gradually decreases. The results of the experimental tests and simulation in subsection “Preliminary control comparison” indicate that the control effectiveness of the piecewise controller is always better than the fuzzy controller. High efficiency of the proposed piecewise controller is verified.

Figure 20 presents the comparison of the root mean square (RMS) values of the acceleration at different rotational speeds. The detailed data are listed in Table 3. When at the idle speed (800 r/min), the vibration acceleration under the fuzzy controller and the piecewise controller decreases by 22.4% and 34.7%, respectively. While at low rotational speed (1400 r/min), the acceleration decreases by 9.9% and 21.3%, respectively. The acceleration decreases by 3.3% and 10.2% at medium rotational speed (1800 r/min), and the acceleration only decreases by 0.3% and 2.5% at high rotational speed (2200 r/min). The reasonable performance of the MR mount system on engine vibration isolation at low frequencies is verified again.

Figure 21(a)–(d) present the applied current at different rotational speeds under the fuzzy controller and the piecewise controller, respectively. Comparing Figure 21(a) and (b), the applied current shows a relationship with not only the rotational speed but also with the vibration acceleration. That is to say, the applied current decreases with the increase of the second-order frequency and rotational speeds. However, the applied current under piecewise controller only related to the rotational speeds (or the vibration frequency), whose values are 2 A at low frequencies, 1 A at medium frequencies, and 0.5 A at high frequencies. It agrees well with the control rules listed in Table 2.

Figures 22 and 23 present response of the accelerations in the time and frequency domains when under

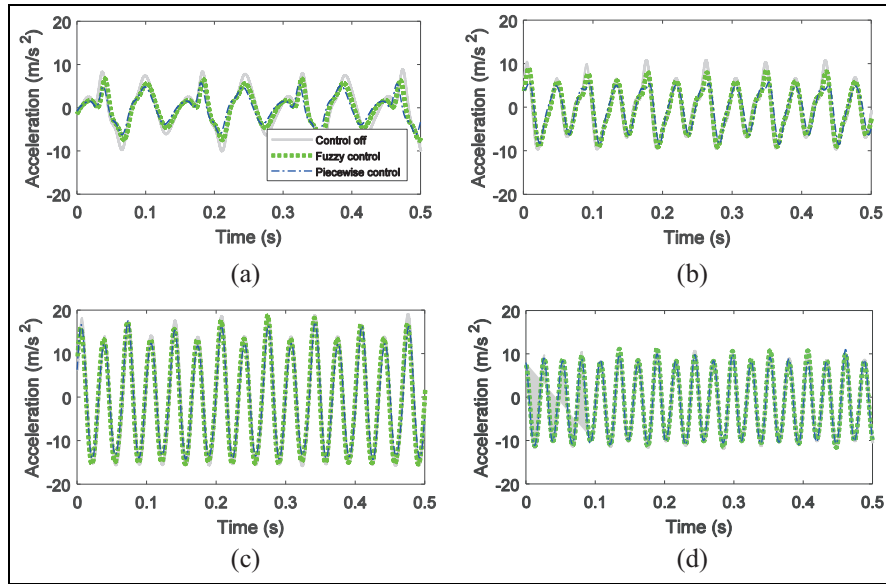


Figure 18. Experimental results of the time histories of the acceleration: (a) 800 r/min, (b) 1400 r/min, (c) 1800 r/min, and (d) 2200 r/min.

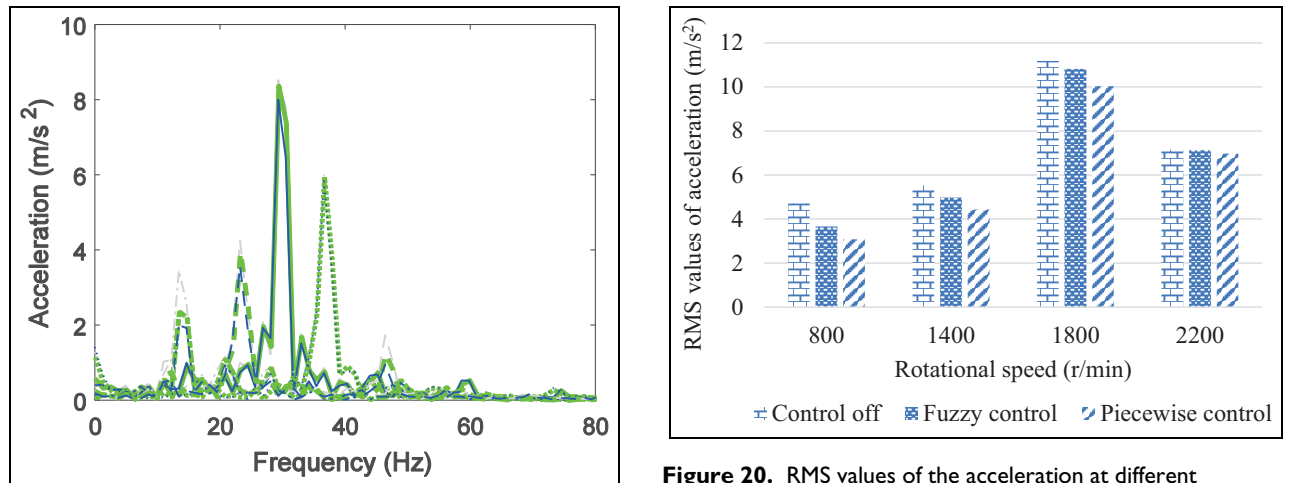


Figure 19. Experimental results of the frequency response of the accelerations when under different strategies and rotational speeds.

Note: Dash-dot line - 800 r/min; Dashed line - 1400 r/min; Solid line - 1800 r/min; and Dotted line - 2200 r/min. Grey - Control off; Green - Fuzzy control; Blue - Piecewise control.

startup and shutdown states. It is seen from results that vibration suppression can be realized under any controller and any conditions. In comparison, the piecewise controller provides a better vibration isolation performance than the fuzzy controller, and the vibration displacement is significantly suppressed. Relative to the passive state at the startup state, the RMS values of the acceleration under the piecewise controller and the fuzzy controller decrease by 67.4% and 33.6%, respectively. Similarly, improvement percentages of 70.0% and 55.0% of the piecewise controller and the fuzzy controller over the passive one at the shutdown condition can be seen from the figure. When in

frequency domain, the vibration at the peak frequency is suppressed effectively under control. Again, the results of the piecewise controller are always better than the fuzzy controller in the full frequency range.

According to the experimental tests, the proposed controller greatly meets the requirements in vibration isolation of the mount system. When at low frequencies with large excitation amplitudes, the mount shows the characteristic of large dynamic stiffness and damping so as to effectively isolate the vibration and reduce the vibration displacement of the engine. When at high frequencies with small excitation amplitudes, the mount has small dynamic stiffness and damping to attenuate high-frequency noises and reduces the vibration transmitted from the engine to the frame. In other words, the dynamic stiffness and damping of the developed MRM-IB can be improved by increasing the applied current at low frequencies with large excitation

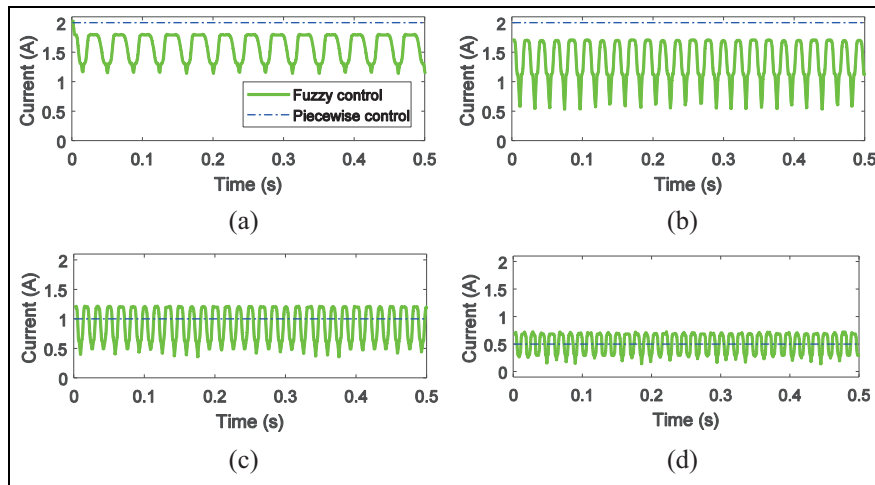


Figure 21. Applied current in the developed MRM-IB: (a) 800 r/min, (b) 1400 r/min, (c) 1800 r/min, and (d) 2200 r/min.

Table 3. RMS value of the acceleration when under different rotational speeds and improvement percentage of the two controllers relative to the passive state.

RMS (m/s^2)	Rotational speed (r/min)			
	800	1400	1800	2200
Control off (passive)	4.7162	5.5216	11.1772	7.1458
Fuzzy control	3.6583	4.9725	10.8123	7.1241
Improvement percentage	+ 22.4%	+ 9.9%	+ 3.3%	+ 0.3%
Piecewise control	3.0807	4.3430	10.0349	6.9646
Improvement percentage	+ 34.7%	+ 21.3%	+ 10.2%	+ 2.5%

RMS: root mean square.

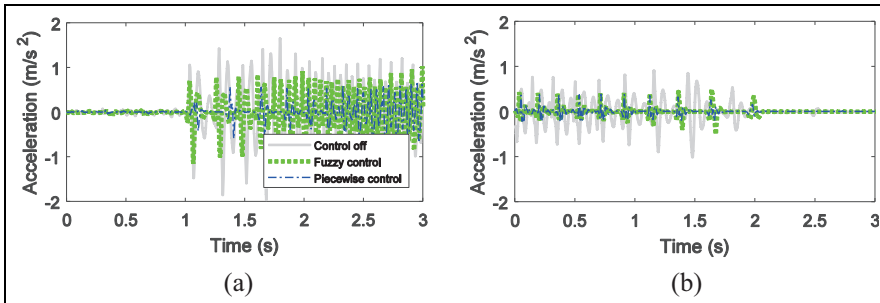


Figure 22. Experimental results of the time histories of the acceleration when under different conditions: (a) startup and (b) shutdown.

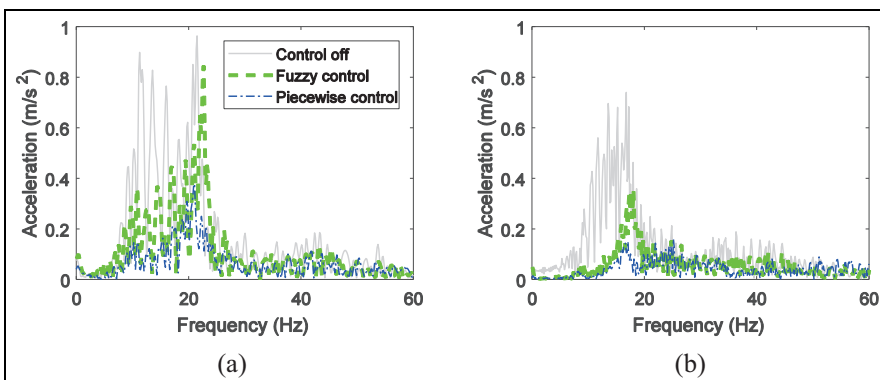


Figure 23. Experimental results of the frequency response of the acceleration when under different conditions: (a) startup and (b) shutdown.

amplitudes. When at high frequencies with small excitation amplitudes, the developed MRM-IB keeps in a passive state, whose dynamic stiffness and damping should be as small as possible. Due to the division of the fuzzy sets and the influence of the acceleration, fuzzy controller cannot output a constant current according to the frequency response characteristics of the engine. It is the reason why the vibration isolation of fuzzy controller is less effective than the frequency-based piecewise controller.

Conclusion

Engine is the source of vehicle power, vibration and noise, and it has properties of wide range of frequency, large excitation velocity, uncertain vibration amplitude and multiple main frequencies of vibration. In order to attenuate or isolate the vibration transmitted from the engine to the vehicle frame or body, mount systems are applied to the connection of the engine and the vehicle frame or body, which not only supports the engine but also promotes the ride comfort property by reducing the acceleration transmissibility from the engine to the vehicle frame and body. Characteristics of the conventional rubber or hydraulic passive mount cannot be actively adjusted to meet the requirement of wide band vibration isolation.

To solve the problem of the existing MR mounts with limited controllable range of dynamic stiffness, large field-off dynamic stiffness and limited working stroke, a MRM-IB was proposed and investigated in this paper. With an identical MR mount geometries or the volume of MR fluids, the MRM-IB provides large controllable range of dynamic stiffness, small field-off dynamic stiffness and large working stroke. The MR fluid channel is formed by the inner and outer concentric cylinders, and the piston divides the inner cylinder. Electromagnetic coils are wound on the grooves of the outside of the inner cylinder. The continuous adjustment of the damping or dynamic stiffness is realized by tuning the applied current in the coils. The structural principle of the developed MRM-IB was verified via the finite element analysis. The MR fluid channel can be guaranteed to satisfy both the large range controllable damping and the requirement of the frequency-insensitive dynamic stiffness. The main rubber spring was verified to be nearly frequency-independent and the influence of the amplitude, current and frequency on the dynamic stiffness and equivalent damping was also studied. An engine excitation model was established and a fuzzy controller and a frequency-based piecewise controller were designed, and then simulations were implemented via MATLAB/Simulink and bench tests. Both the fuzzy controller and the piecewise controller could isolate the vibration of the engine at full frequency range. As compared with the fuzzy controller, the piecewise controller is more effective for engine vibration control. Finally, the

experimental tests based on the test bench of the engine vibration isolation of the developed MRM-IB was carried out. When the second-order frequency is 13.3 Hz, the RMS values under the piecewise controller and the fuzzy controller decrease by 34.7% and 22.4%, respectively. When the second-order frequency is 23.3 Hz, the RMS values decrease by 21.4% and 9.9%, respectively. The RMS values decrease by 10.2% and 3.3%, respectively, when the second-order frequency is 30 Hz. The RMS values decrease by 2.5% and 0.2%, when the second-order frequency is 36.7 Hz, respectively. The same results with the simulations, the two controllers are effective in the full frequency range, especially at low frequencies. In addition, the two controllers were compared and analyzed at both startup and shutdown states. As compared with the passive mount system during start condition, the RMS values of the acceleration under the piecewise controller and the fuzzy controller decrease by 67.4% and 33.6%, respectively. Furthermore, during the shutdown condition, the RMS values decrease by 70.0% and 55.0%, respectively.

Declaration of conflicting interests

The author(s) declared no potential conflicts of interest with respect to the research, authorship, and/or publication of this article.

Funding

The author(s) disclosed receipt of the following financial support for the research, authorship, and/or publication of this article: The authors wish to acknowledge the financial support from Tai'an Special Vehicle Co., Ltd (Project No. W2020JSKF0060).

ORCID iD

Xian-Xu ‘Frank’ Bai  <https://orcid.org/0000-0003-4477-8335>

References

1. Ahamed R, Choi SB and Ferdous MM. A state of art on magneto-rheological materials and their potential applications. *J Intell Mater Syst Struct* 2018; 29: 2051–2095.
2. Bai XX, Cai FL and Chen P. Resistor-capacitor (RC) operator-based hysteresis model for magnetorheological (MR) dampers. *Mech Syst Signal Pr* 2019; 117: 157–169.
3. Christie MD, Sun S, Deng L, et al. A variable resonance magnetorheological-fluid-based pendulum tuned mass damper for seismic vibration suppression. *Mech Syst Signal Pr* 2019; 116: 530–544.
4. Cheng H, Wang M, Liu C, et al. Improving sedimentation stability of magnetorheological fluids using an organic molecular particle coating. *Smart Mater Struct* 2018; 27: 075030.
5. Eshaghi M, Sedaghati R and Rakheja S. Vibration analysis and optimal design of multi-layer plates partially treated with the MR fluid. *Mech Syst Signal Pr* 2017; 82: 530–544.

6. Li Z, Liao C, Fu B, et al. Study of radial flow mode magnetorheological energy absorber with center drain hole. *Smart Mater Struct* 2018; 27: 105008.
7. Maddah AA, Hojjat Y, Karafi MR, et al. Reduction of magneto rheological dampers stiffness by incorporating of an eddy current damper. *J Sound Vib* 2017; 396: 51–68.
8. Dutta S and Chakraborty G. Performance analysis of nonlinear vibration isolator with magneto-rheological damper. *J Sound Vib* 2014; 333: 5097–5114.
9. Nguyen T, Elahinia M and Wang S. Hydraulic hybrid vehicle vibration isolation control with magnetorheological fluid mounts. *Int J Veh Des* 2013; 63: 199–222.
10. Nguyen TM, Ciocanel C and Elahinia MH. A squeeze-flow mode magnetorheological mount: design, modeling, and experimental evaluation. *J Vib Acoust* 2012; 134: 021013.
11. Barber DE and Carlson JD. Performance characteristics of prototype MR engine mounts containing glycol MR fluids. *J Intell Mater Syst Struct* 2010; 21: 1509–1516.
12. Mansour H, Arzanpour S, Golnaraghi MF, et al. Semi-active engine mount design using auxiliary magnetorheological fluid compliance chamber. *Veh Syst Dyn* 2011; 49: 449–462.
13. Phu DX, Shah K and Choi SB. A new magnetorheological mount featured by changeable damping gaps using a moved-plate valve structure. *Smart Mater Struct* 2014; 23: 125022.
14. Nguyen QH, Choi SB, Lee YS, et al. Optimal design of high damping force engine mount featuring MR valve structure with both annular and radial flow paths. *Smart Mater Struct* 2013; 22: 115024.
15. Nguyen QH, Phu DX, Park JH, et al. Development of high damping magneto-rheological mount for ship engines. *Appl Mech Mater* 2013; 336: 953–959.
16. Han C, Choi SB, Lee YS, et al. A new hybrid mount actuator consisting of air spring and magneto-rheological damper for vibration control of a heavy precision stage. *Sens Actuat A Phys* 2018; 284: 42–51.
17. Yang SY, Han C, Shin CS, et al. Dynamic characteristics of passive and semi-active cabin mounts for vibration control of a wheel loader. *Int J Heavy Veh Syst* 2019; 26: 239–261.
18. Li Z, Zhang X, Guo K, et al. A novel squeeze mode based magnetorheological valve: design, test and evaluation. *Smart Mater Struct* 2016; 25: 127003.
19. Farjoud A, Ahmadian M, Mahmoodi N, et al. Nonlinear modeling and testing of magneto-rheological fluids in low shear rate squeezing flows. *Smart Mater Struct* 2011; 20: 085013.
20. Chen P, Bai XX and Qian LJ. Magnetorheological fluid behavior in high-frequency oscillatory squeeze mode: experimental tests and modelling. *J Appl Phys* 2016; 119: 105101.
21. Chen P, Bai XX, Qian LJ, et al. A magneto-rheological fluid mount featuring squeeze mode: analysis and testing. *Smart Mater Struct* 2016; 25: 055002.
22. Sapiński B and Snamina J. Automotive vehicle engine mount based on an MR squeeze-mode damper: modeling and simulation. *J Theor Appl Mech* 2017; 55: 377–388.
23. Yoo JH and Wereley NM. Design of a high-efficiency magnetorheological valve. *J Intell Mater Syst Struct* 2002; 13: 679–685.
24. Phillips RW. *Engineering applications of fluids with a variable yield stress*. PhD Dissertation, University of California, Berkeley, CA, 1969.
25. Bai XX and Chen P. On the hysteresis mechanism of magnetorheological fluids. *Front Mater* 2019; 6: 36.

Appendix I

Notation

A_p	the effective area of the piston
B	the magnetic flux density
c	the equivalent damping of the MRM-IB
f	the main frequency of the engine
f_2	the second-order frequency of the engine
F	the output force of the MRM-IB
F_j	the resultant force
F_s	the force of the main rubber spring
i	the applied current
k	the stiffness of the MRM-IB
L	the length of the MR fluid channel
m	the engine mass
m_j	the equivalent mass converted to the piston pin
m_r	the equivalent mass converted to the crankshaft pin
Q_z	the reciprocating inertial force on the piston pin
Q_{rv}	the rotating inertial force on the crankshaft pin
r	the length of the crankshaft
t	the time
$x, \dot{x},$ and \ddot{x}	the vibration displacement, velocity and acceleration of the engine
\dot{x}_r and \ddot{x}_r	the flow velocity and acceleration of the MR fluids in the channel
ΔL	the width of the electromagnetic coil winding
ΔP	the total pressure drop through the piston
$\Delta P_1, \Delta P_\tau, \Delta P_\eta$	the pressure drop caused by the inertia, the MR effect and the viscosity
ΔR	the width of the MR fluid channel
τ_y	the shear yield stress of the MR fluids
η	the field-off viscosity of the MR fluids
ρ	the density of the MR fluids
λ	the length ratio of the crankshaft to the connecting rod
ω	the angular speed of rotating crankshaft